Methods 128 (2017) 119–128

Contents lists available at ScienceDirect

Methods

journal homepage: www.elsevier.com/locate/ymeth

Imaging chemistry inside living cells by stimulated Raman scattering microscopy

Hyeon Jeong Lee [a,b], Ji-Xin Cheng [a,b,c,d,*]

[a] Weldon School of Biomedical Engineering, Purdue University, West Lafayette, IN 47907, USA
[b] Interdisciplinary Life Science Program, Purdue University, West Lafayette, IN 47907, USA
[c] Department of Chemistry, Purdue University, West Lafayette, IN 47907, USA
[d] Photonics Center, Boston University, Boston, MA 02215, USA

ARTICLE INFO

Article history:
Received 25 March 2017
Received in revised form 6 June 2017
Accepted 20 July 2017
Available online 23 July 2017

Keywords:
Chemical imaging
Stimulated Raman scattering microscopy
Vibrational spectroscopy
In vivo imaging
Raman tag

ABSTRACT

Stimulated Raman scattering (SRS) microscopy is a vibrational imaging platform developed to visualize chemical content of a biological sample based on molecular vibrational fingerprints. With high-speed, high-sensitivity, and three-dimensional sectioning capability, SRS microscopy has been used to study chemical distribution, molecular transport, and metabolic conversion in living cells in a label-free manner. Moreover, aided with bio-orthogonal small-volume Raman probes, SRS microscopy allows direct imaging of metabolic activities of small molecules in living cells.

© 2017 Elsevier Inc. All rights reserved.

Contents

Abbreviations: CRS, coherent Raman scattering; SRG, stimulated Raman gain; SRL, 3D, three-dimensional; SRS, stimulated Raman scattering; TPEF, two-photon excitation fluorescence; OPO, optical parametric oscillator; AOM, acousto-optic modulator; EOM, electro-optic modulator; PCA, principle component analysis; MCR, multivariate curve resolution; H&E, hematoxylin and eosin; *C. elegans*, *Caenorhabditis elegans*; DMSO, dimethyl sulfoxide; C–D, carbon-deuterium.

* Corresponding author at: Photonics Center, Boston University, Boston, MA 02215, USA.
E-mail address: jxcheng@bu.edu (J.-X. Cheng).

http://dx.doi.org/10.1016/j.ymeth.2017.07.020
1046-2023/© 2017 Elsevier Inc. All rights reserved.

1. Introduction

A central theme of chemical science is deciphering how molecules function in a complex system, such as a living cell. Such study contributes to the society by providing fundamental knowledge in medical science to improve our lives. Yet, our understanding of chemistry in living system (e.g., how intensive biosynthetic chemical activity drives cell development, function, and inter-cellular communications) is still limited, partly because conventional biochemical assays treat the cell, a highly dynamic structure, as a static bag of molecules. In current paradigms, molecules are extracted from a tissue and analyzed by various analytical techniques such as immunoblotting and liquid chromatography/mass spectrometry. These *in vitro* assays provide very little information about the spatial distribution or temporal dynamics of molecules in real life, thus they are unable to tell the exact roles of molecular activities on cellular functions [1]. Furthermore, the molecular profile of a cell may alter during the extensive sample processing procedures. For *in situ* imaging, fluorescent microscopy is widely used. By measuring fluorescent signals from endogenous species, such as coenzymes nicotinamide adenine dinucleotide (NADH) and Flavin adenine dinucleotide (FAD), cell metabolism can be measured in real time [2–4]. Unfortunately, not all endogenous molecules possess the ideal optical properties. Fluorescent labels allow imaging of proteins and some key metabolites in living cells, but they often disturb the function of small biomolecules, such as glucose and cholesterol, limiting the ability to monitor their activities. These limitations stress the critical need of establishing new platforms for learning chemistry *in situ* in living systems.

Raman-scattering based vibrational spectroscopy has been a powerful tool for non-invasive, label-free analysis of chemicals. Raman scattering is an inelastic scattering process, in which an excitation photon loses energy to a certain molecular vibration mode, resulting a scattered photon with a different wavelength. Such energy losses are directly related to vibrational transitions of a molecule, showing as peaks in Raman spectrum (Fig. 1a). Therefore, analysis of Raman-scattered photons can be used to identify chemical species quantitatively. Raman microscope, which is now commercially available, allows chemical imaging with submicron spatial resolution [1]. However, because Raman scattering is a feeble process, the image acquisition speed of current Raman microscopes (at least tens of minutes per frame) is insufficient to follow chemical dynamics *in vivo*. To improve the imaging speed, line illumination has been adopted for ultra-fast Raman imaging, allowing several minutes per frame imaging speed (Nanophoton, Osaka, Japan). To overcome the speed limitation, coherent Raman scattering (CRS) microscopy [5] has been developed to enhance the Raman signal level. In CRS microscopy, two excitation beams, known as pump (ω_p) and Stokes (ω_s), are used. When the laser-beating frequency ($\omega_p - \omega_s$) is in resonance with a molecular vibration frequency (Ω), four major CRS processes occur simultaneously, known as coherent anti-Stokes Raman scattering (CARS), coherent Stokes Raman scattering, stimulated Raman gain (SRG), and stimulated Raman loss (SRL) (Fig. 1b). These nonlinear optical processes offer a large signal that allows live-cell imaging at a speed three to four orders of magnitude faster than Raman microscope. As nonlinear optical process, CARS and SRS microscopy offers inherent three-dimensional (3D) sectioning capability. Fur-

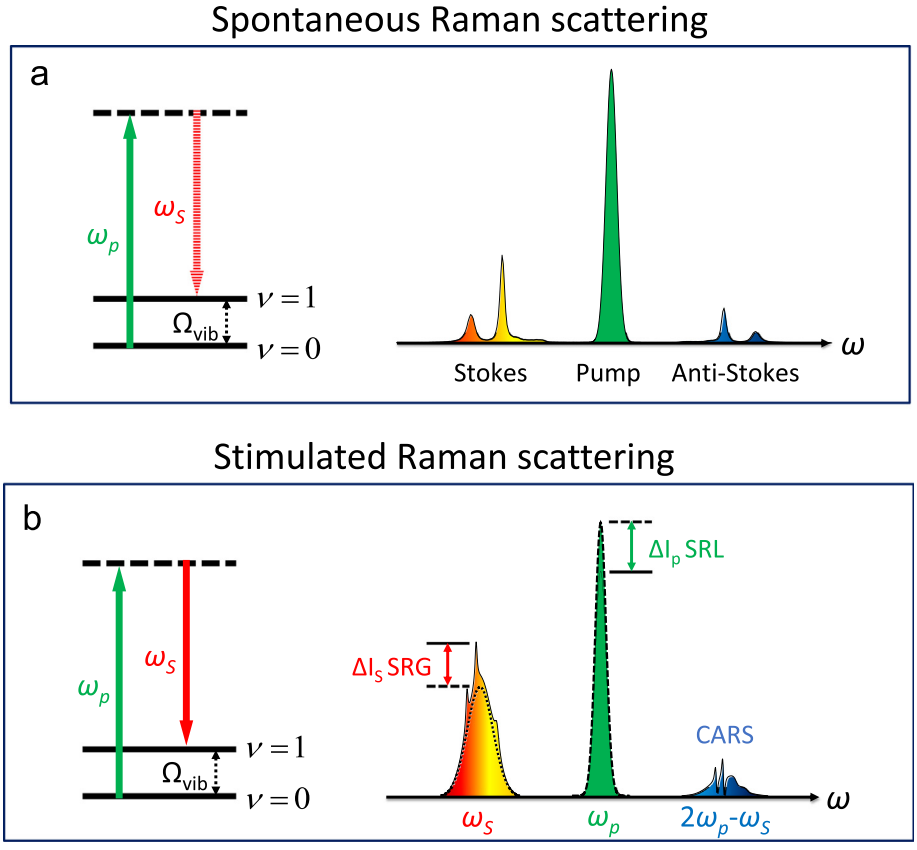

Fig. 1. Spontaneous and coherent Raman scattering processes. (a) Energy diagram of spontaneous Raman scattering and representative spectra. (b) Energy diagram of SRS and CARS processes and representative spectra. Broadband coherent Raman scattering induced by a pump field at ω_p and a Stokes field at ω_S. Solid arrows indicates laser excitation and dashed arrow indicates the spontaneous scattering process Ω_{vib} denotes the vibrational energy.

thermore, because CRS microscopy uses near infrared light for excitation, it induces minimal photodamage to cells.

CARS is a four-wave mixing process in which the signal is generated at a higher frequency (Fig. 1b). CARS signal consists of a non-resonant part independent of the beating frequency and a resonant part depending on the beating frequency. The non-resonant background part is contributed by electronic motions [6,7]. SRG and SRL belong to stimulated Raman scattering (SRS) [8]. It is a dissipative process accompanied by intensity increase in the Stokes beam and intensity decrease in the pump beam when the energy difference between the two beams pumps the molecule from a ground state to a vibrationally excited state (Fig. 1b). Because SRG and SRL signals appear at the same frequency as the incident beams, optical modulation and demodulation are used to extract those signals. In contrast to CARS, SRS signal is free of non-resonant background, spectral distortion, and is linearly dependent on molecular concentration. These advantages allow SRS microscopy to study lipids, proteins, nucleic acids, glucose, and other metabolites in living cells and organisms via quantitative chemical imaging with high sensitivity [9,10]. In accordance with the rapid development of SRS microscopy field, there is number of reviews on application of SRS imaging in living cells and/or biomedical research [11–16]. In this paper, we discuss different SRS imaging modalities and their applications to study chemical content, transport, and reaction in biological samples.

2. SRS imaging modalities

Key components of a SRS microscope include a two-color laser source, an optical modulator, a laser scanner, a detector and an electronic demodulator (Fig. 2). Below we will review recently developed approaches of constructing a SRS microscope.

2.1. Single-frequency SRS imaging

In single-frequency SRS imaging scheme, the laser energy is focused to a specific Raman mode of typical bandwidth around 10–100 cm^{-1}. To achieve high spectral resolution, picosecond laser is preferred, especially for imaging narrow Raman bands. At the same time, picosecond excitation reduces cross-phase modulation background and photodamage. However, SRS is a nonlinear process, which requires high peak power to generate signals, and the signal level can be increased by more than one order using femtosecond laser [17]. Moreover, femtosecond excitation is preferred when the SRS microscope is coupled with other widely used imaging modalities, such as two-photon excitation fluorescence (TPEF), second harmonic generation, and third harmonic generation. Several laser sources were developed for SRS imaging: (1) electronically synchronized, mode-locked Ti:sapphire lasers which produce mode-locked pulse trains with a repetition rate of ~80 MHz and pulse duration from several picoseconds to 100 femtoseconds [18], (2) a mode-locked picosecond Nd:YVO4 laser at 1064 nm that synchronously pumps a second beam through optical parametric oscillator (OPO) [19], (3) a femtosecond Ti:sapphire laser with an OPO [20].

SRS signal appears at the same frequency as one of the excitation beams. To extract the signal, optical modulation and demodulation are used. Pump or Stokes beam is modulated at megahertz frequency using acousto-optic modulator (AOM) or electro-optic modulator (EOM). These two synchronized laser pulses are spatially overlapped and coupled into a laser scanning microscope. A high numeric aperture objective lens is used for tight focusing. Oil condenser is used to suppress background from cross-phase modulation by enhancing the signal collection efficiency [21]. A photodiode is used for the detector, which can withstand high laser

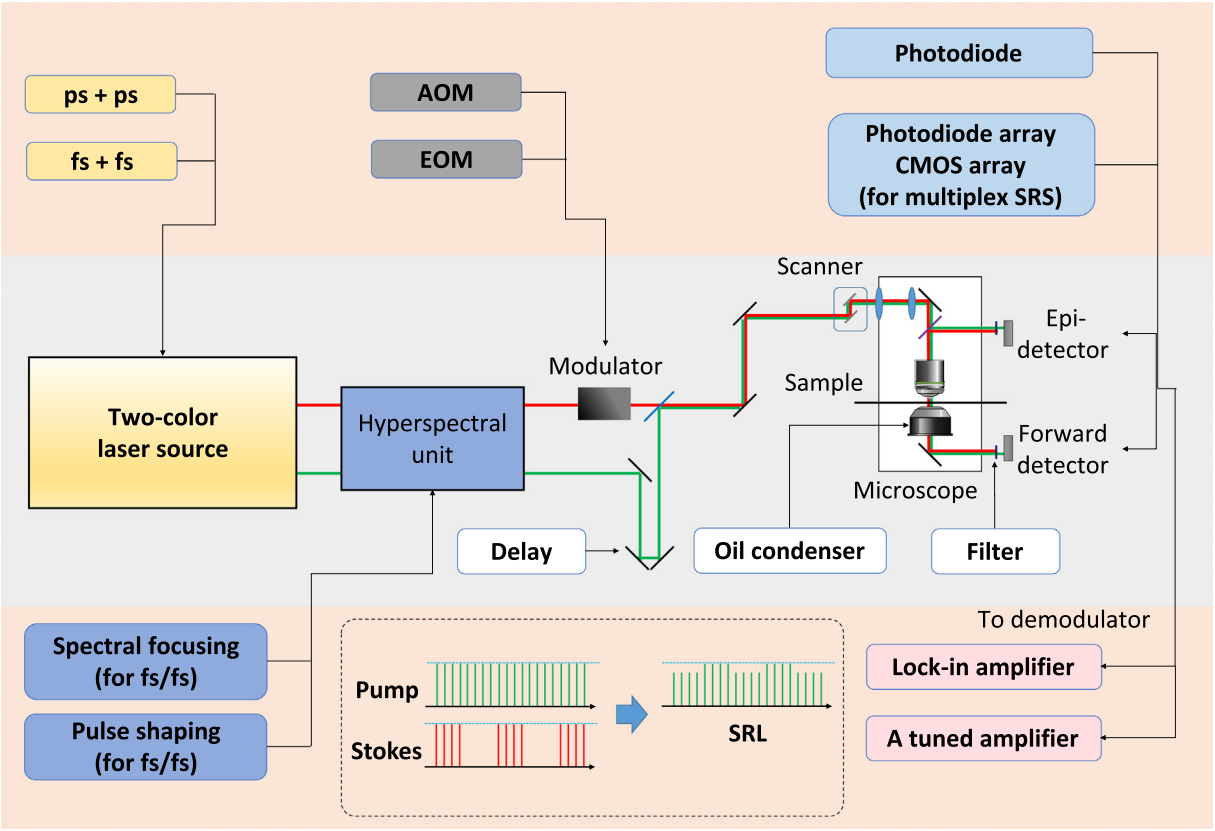

Fig. 2. Instrumentation of SRS microscopy. Insert: Schematic of the pulse trains in the stimulated Raman loss. OPO, optical parametric oscillator; AOM, acousto-optic modulator; EOM, electro-optic modulator; CMOS, complementary metal-oxide-semiconductor.

power at milliwatt level. SRL or SRG signal is extracted with a demodulator, such as a lock-in amplifier. As a cost-effective alternative, a tuned amplifier that resonates at the modulation frequency can also be used as a demodulator [22]. Various SRS imaging setups have been demonstrated based on the abovementioned methods.

2.2. Frame-by-frame hyperspectral SRS imaging

Single-frequency SRS imaging provides real-time chemical imaging based on isolated Raman bands. However, it is difficult to distinguish spectrally overlapped Raman bands. Hyperspectral SRS microscopy offers better chemical specificity. Frame-by-frame hyperspectral SRS imaging records a stack of SRS images at multiple Raman shifts. Wavelength scanning is a straightforward method for hyperspectral SRS imaging. Using two tunable picosecond lasers, the wavelength is tuned over a continuous range to cover multiple Raman shifts [23,24]. The fastest spectral tuning approach can resolve more than 50 spectrally-distinct frames in ~10 min.

With the broad bandwidth, femtosecond lasers can be used for hyperspectral SRS imaging in multiple ways. A relatively simple and robust method utilizes spectral focusing technique [25,26]. In this approach, two femtosecond laser beams are chirped with NSF57 glass to picosecond range, which improves spectral resolution [27]. By tuning the time delay between the two chirped pulses, the frequency difference is subsequently changed to excite different Raman shifts. With this approach, hyperspectral SRS images can be recorded within a minute over a ~270 cm^{-1} spectral window. The important optimization parameters for this method are linear chirping and alignment of beams and calibration of Raman shift. Another approach uses a pulse shaper to filter and scan a narrow spectral component out of a broadband femtosecond spectrum [28–30]. Using spectral filtering coupled with a customized fiber amplifier, a hyperspectral SRS imaging of spectral resolution better than 10 cm^{-1} can be reached [31].

2.3. Multiplex SRS imaging

Hyperspectral SRS imaging generally takes seconds to minutes to obtain the hyperspectral SRS image stacks. This acquisition speed causes spectral and spatial distortions when imaging dynamic process happening *in vivo*. Multiplex SRS microscopy was developed to provides high-speed high-content biological imaging. Multiple Raman bands can be detected simultaneously in the spectral domain or in the time domain. The main requirement for multiplex SRS microscopy in spectral domain is parallel detection of dispersed SRS signals. The detection using a photodiode array has been demonstrated by Marx et al. [32]. To extract the signal, demodulators are required, such as a high-frequency lock-in amplifier. Lu et al. used three independent lock-in amplifiers to demonstrate multicolor SRS imaging [33]. A multichannel lock-in amplifier has been developed for 128-channel multiplex SRS microscopy [34]. Resonant amplifiers [22] provide cost-effective approach for multiplex detection, and by designing a 32-channel tuned-amplifier array integrated with a photodiode array, Liao et al. significantly reduced the spectral acquisition time to 32 μs with a spectral window of ~200 cm^{-1} [35].

Another approach in time domain utilizes frequency coding. In this approach, each photon is modulated at certain frequency, which is then collected by a single detector. The spectral information is extracted by demodulating at different frequencies. Fu et al. [36] demonstrated parallel detection of three-color SRS imaging by modulating each color of the excitation laser with an acousto-optical tunable filter at a specific kilohertz-rate frequency. Megahertz-rate modulation has been demonstrated by scanning dispersed excitation beam on a spatial pattern inside a femtosecond pulse shaper, achieving a spectral acquisition within 60 μs per pixel [37].

2.4. Image analysis

Hyperspectral SRS microscopy generates x-y-Ω image stacks. By extracting spectral profile at each pixel, concentration maps of different species can be generated. Several imaging processing methods are available for analyzing hyperspectral SRS image stacks, including principle component analysis (PCA) [25], multivariate curve resolution (MCR) [28], and spectral phasor analysis [38]. PCA is used to determine the number of principle components in the hyperspectral image stack. MCR analysis is a widely-applied method to analyze hyperspectral SRS images [28,39,40]. It decomposes the SRS image stack into concentration profiles (matrix C) and spectra of each component (ST). The dataset D and the reference spectra of each component are entered in the model $D = C \cdot ST + E$, in which S contains the output spectra of all fitted components, and T is the transpose of matrix S. E is the residual matrix or experimental error. Initial estimate of pure spectra can be obtained from PCA, k-means clustering or prior knowledge of the sample, and with this information, an alternating least squares algorithm calculates C and S iteratively until optimal fit to the data matrix D is achieved. The output is a concentration map for every principle component, expressed as a percentage relative to the intensity of the MCR-optimized spectrum.

3. Imaging chemistry in cells and tissues by label-free SRS microscopy

Label-free SRS imaging has been applied to *in vivo* imaging of mouse skin [8,35–37,41], brain [42], *Caenorhabditis elegans* (*C. elegans*) [39,43,44], *Drosophila* [45,46], tadpoles [47], and human cancer tissues [48–50]. C—H bond is the most abundant chemical bond in living cells, providing chemical information of molecules, such as lipids and proteins. Compared to C—H region where multiple C—H stretching bands are highly crowded and spectrally overlapped, fingerprint region (500–1800 cm^{-1}) is used to provide better chemical specificity for imaging of nucleic acids, metabolites, and drugs. Below we will review applications of SRS imaging to study chemical content, dynamics and functions in living cells, tissues, and human samples.

3.1. Mapping chemical content in cells and tissues

Altered lipid metabolism is recognized as a signature of various types of human cancer. Although intracellular lipid accumulation has been observed in human cancer tissues and cells, it has not been widely used as a prognostic factor or therapeutic target due to limited understanding of lipid metabolism in cancer. In particular, the role of lipid accumulation in cancer progression remains elusive partly because lack of tool for mapping lipid species in a single-cell level. Quantitative analysis of lipid content at single-cell level in human patient cancerous tissue by coupling confocal Raman microscopy with SRS microscopy enabled identification of metabolic signature of aggressive human prostate cancer [48]. The spectroscopic imaging data revealed aberrant accumulation of cholesteryl ester in lipid droplets of high-grade prostate cancer and metastases (Fig. 3a), which was shown to be a consequence of loss of tumor suppressor PTEN and subsequent activation of PI3K/AKT pathway in prostate cancer cells. Depleting cholesteryl ester storage significantly suppressed tumor growth in mouse xenograft models and impaired cancer invasion [48]. This work opens opportunities for using altered cholesterol metabolism for

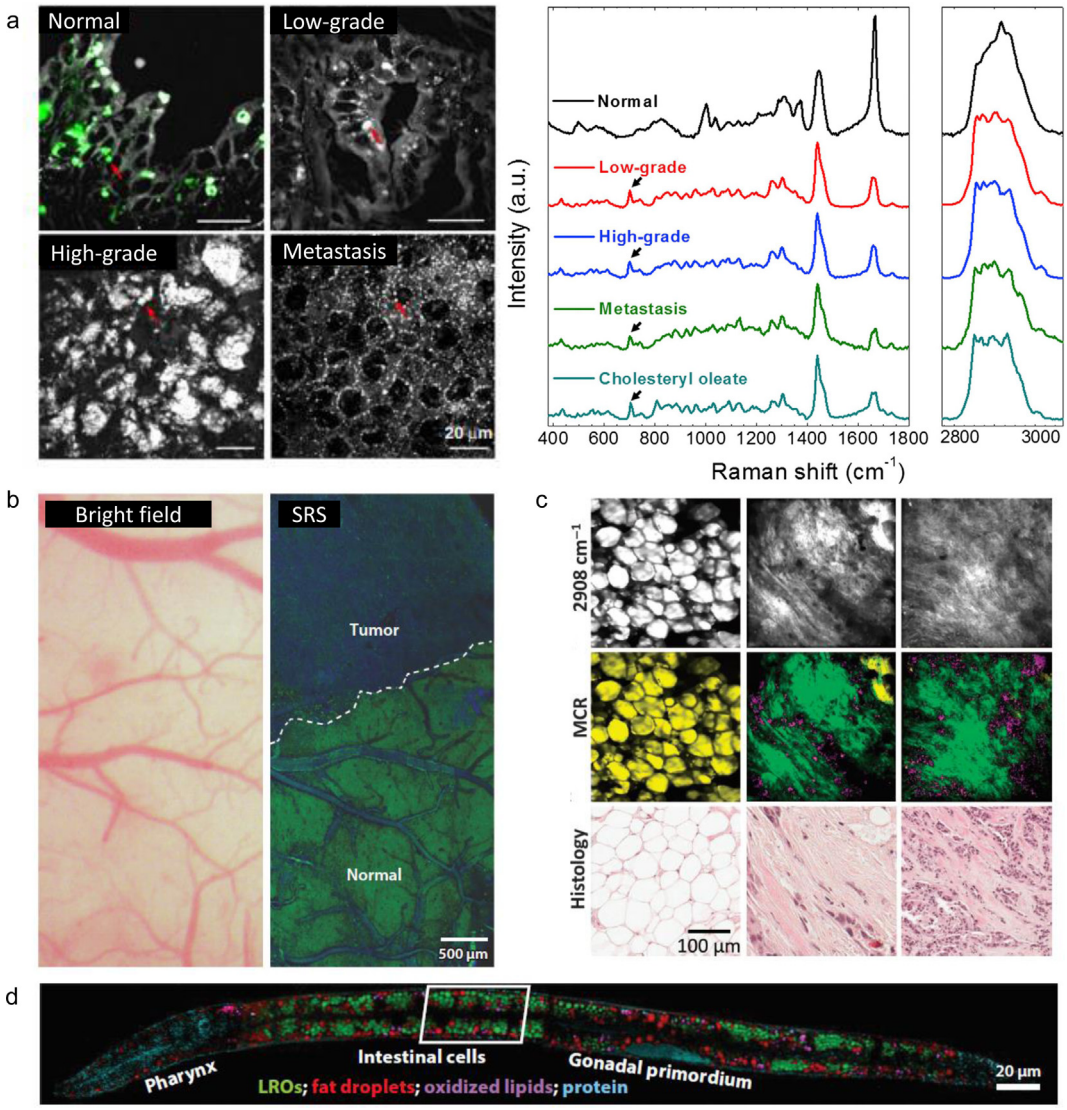

Fig. 3. Mapping chemical content in cells and tissues. (a) SRS and two-photon fluorescence images of normal prostate, low-grade, high-grade, and metastatic prostate cancers, respectively. Autofluorescent granules and lipid droplets are indicated by red arrows (gray, SRL; green, two-photon fluorescence). Raman spectra of autofluorescent granules in normal prostate, lipid droplets in prostate cancers, and pure cholesteryl oleate. Spectral intensity was normalized by CH_2 bending band at 1442 cm^{-1}. Black arrows indicate the bands of cholesterol rings at 702 cm^{-1}. Reprinted with permission from Ref. [48]. (b) Bright-field image and SRS image showing normal brain-tumor interface (dashed line). Reprinted with permission from Ref. [42]. (c) SRS images of a cancerous bulk human breast tissue after MCR analysis and H&E stained histologic result of the same tissue. Reprinted with permission from Ref. [37]. (d) Quantitative mapping of neutral fat droplets, lysosome-related organelles (LROs), oxidized lipids, and protein in the whole *C. elegans* worm with daf-2 mutant. Reprinted with permission from Ref. [39]. (For interpretation of the references to color in this figure legend, the reader is referred to the web version of this article.)

prostate cancer diagnosis and treatment. Recently, by hyperspectral SRS imaging of single living cells, Li et al. [49] identified lipid unsaturation level as a metabolic marker for ovarian cancer stem cells. By analysis of ratio between 3002 cm^{-1} and 2900 cm^{-1} from the hyperspectral SRS image-stacks, lipid unsaturation levels were mapped in the individual cells, revealing high unsaturation level in cancer stem cell population. This signature was shown to be directly regulated by NF-κB and inhibiting lipid desaturation effectively eliminated cancer stem cells, which blocked tumor initiation capability *in vivo* [49]. This work demonstrates the importance of single-cell chemical imaging, which enabled label-free identification of rare and the most malignant population of cancer cells and cancer stem cell-specific therapy.

At the tissue level, *in situ* mapping of chemical content allowed visualization of cholesterol crystals, lipids, proteins, and nucleic acids. By separating sterol C=C band at 1669 cm^{-1}, acyl C=C band 1655 cm^{-1} and broad amide I band, the distribution of cholesterol crystals, lipids and proteins were mapped in an intact atherosclerotic arterial tissue [51]. CH_2 and CH_3 stretching modes represent major components of lipid and protein, respectively, and are used to map these two compositions in fresh mouse ear skin [33] and *ex vivo* mouse skin tissue [36]. Nucleic acid has signature Raman peaks at 785 cm^{-1} and 1090 cm^{-1}, which was used to study the distribution of nucleic acid in mammalian cells and single salivary gland cells of *Drosophila* larvae [46].

For medical application, label-free histology by SRS imaging demonstrates one of the important translational applications of this imaging platform [37,42,50,52]. Histopathology is a standard examination for diagnosis. However, the current techniques require the tissues to be frozen or fixed and stained with dyes before they can be observed, which is label-intensive and time-consuming. By analysis of SRS images at 2850 cm^{-1} and 2930 cm^{-1} for CH_2 and CH_3 vibration modes, Freudiger et al. [52] showed stain-free histopathological imaging of fresh tissue, which

is comparable to a hematoxylin and eosin (H&E) staining. Using this approach, *in vivo* SRS imaging of mouse brain after craniotomy was performed to locate brain tumor margin [42] (Fig. 3b). More recently, Lu et al. [50] profiled a range of human brain tumors from patients to establish hallmarks for glioma classification. Owing to the sharp contrast between lipids and proteins provided by SRS imaging, vascular proliferation, red blood cells and necrosis were easily discriminated. Moreover, marked alteration of myelinated fibers observed using SRS imaging of fresh oligodendroglioma suggested a new mechanism for tumor to modify microenvironment for adaptive advantage [50]. A recent development of spectrometer-free multiplex SRS microscopy further enabled *in situ* label-free histological analysis of highly scattered, 5-mm-thick human breast cancer tissues [37] (Fig. 3c). This work opens opportunities to perform *in vivo* clinical imaging using label-free SRS microscopy for cancer diagnosis and tumor margin detection during the surgery.

Chemical mapping in model organisms such as *C. elegans* has been widely applied to study metabolic process. Identifying genetic regulators of fat storage has been challenging due to controversies of the visualization tool for lipids [53,54] and complication from quantification of fluorescence labeling and dye-incorporation into lipids in the organisms. Owing to high peak power, femtosecond excitation was used to increase the SRS signal level and performed label-free 3D sectioning of *C. elegans* to distinguish fat storage from membrane lipids [17]. SRS imaging platform has also been combined with RNAi screening to discover novel genetic regulators of fat storage in *C. elegans* [44]. Mapping chemical content in *C. elegans* by hyperspectral SRS imaging further provided label-free approach to distinguish intracellular compartments, including fat droplets, lysosome-related organelles, oxidized lipids, and proteins [39] (Fig. 3d). By examining spectral profiles in the fingerprint regions using k-means clustering and MCR analysis, the degree of lipid unsaturation and oxidation and cholesterol storage were mapped in the entire worm. This study demonstrates the potential of applying hyperspectral SRS imaging to understand how lipid storage change in response to diet and the role of insulin in obesity, diabetes and longevity in animals.

3.2. Monitoring molecular transport in cells and tissues

One advantage of label-free imaging is the capability of quantitative long-duration imaging. This is especially important when studying the dynamics and tracking changes of biomolecules during ongoing processes, such as embryonic development and injury. Dou et al. [45] performed time-lapse SRS imaging of developing *Drosophila* embryo to track single lipid droplet motion within large populations of droplets (Fig. 4a). By analysis of velocity and turning frequency of each droplet, the mathematical model for the lipid droplet movement was developed to show key regulatory point of lipid droplet dynamics in the developmental process [45]. This work shows a potential of using SRS imaging technique to study lipid trafficking in living cells and organisms. More recently, by *in vivo* SRS imaging of single neurons and myelin in the spinal cord, Hu et al. [47] monitored myelin sheath formation, maturation of a node of Ranvier and myelin degradation in live *Xenopus Laevis* tadpole.

Dynamic information is especially important in the study of drug molecules in living systems because the treatment efficiency is highly dependent on the delivery of drug to the target locations. Several chemical signatures of drug molecules have been used to track drug penetration to skin and drug release inside living cells. Fu et al. characterized chemical signature of a tyrosine-kinase inhibitors, which is used for cancer therapy, to image intracellular distribution. The direct visualization of drug in living cells allowed evaluation of lysosome accusation and release of drug [26]. Others

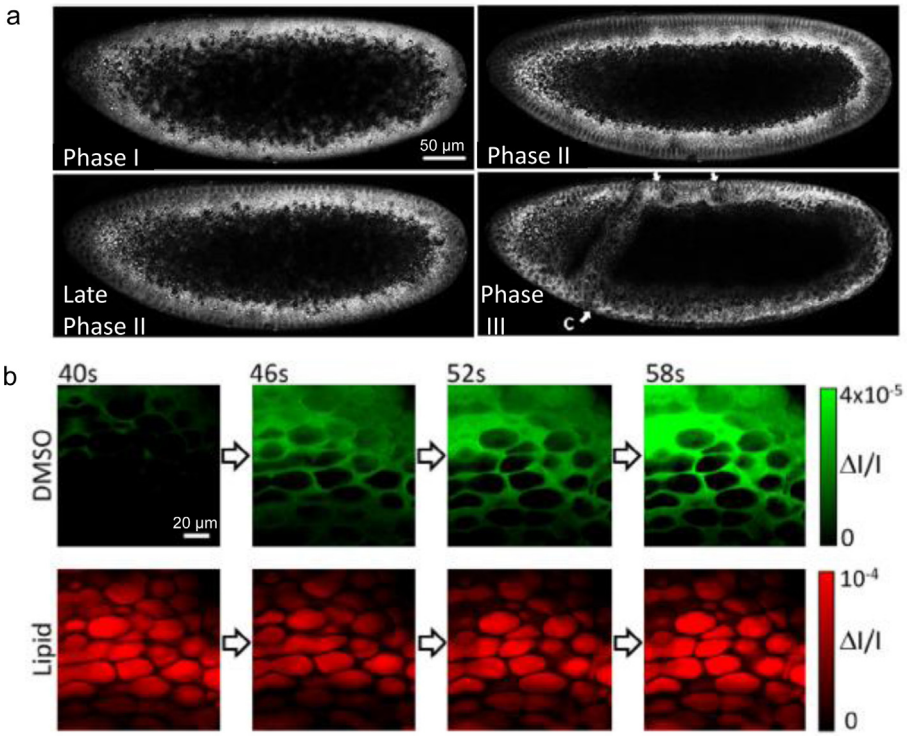

Fig. 4. Monitoring chemical trafficking in cells and tissues. (a) SRS images of a developing *drosophila* embryo in three distinct phases of lipid droplet global distribution. Phase I, before nuclear cycle 13; late phase I, at the interphase of cycle 13; phase II, midcellularization; phase III, gastrulation. Reprinted with permission from Ref. [45]. (b) Time-lapsed concentration maps of DMSO and lipids extracted from multiplex SRS images, showing drug diffusion through mouse skin tissue. Reprinted with permission from Ref. [35].

have demonstrated the tracking of drug molecules penetrating mouse or human skins using *in vivo* SRS imaging [8,41]. By focusing at S=O and C=C bonds, mouse skin uptake of dimethyl sulfoxide (DMSO) and retinoic acid was imaged. More recently, owing to fast spectral acquisition speed, multiplex SRS imaging allowed visualization of DMSO drug diffusion through mouse skin tissues in real-time (Fig. 4b), revealing fast dynamic diffusion process without spectral distortion from the motions of the animal [35]. This is not easily achieved using frame-by-frame hyperspectral SRS imaging. Liao et al. demonstrated *in vivo* SRS imaging of vitamin E distribution on mouse skin by multiplexed modulation at megahertz rate and spectral acquisition within 60 μs per pixel [37].

3.3. Probing chemical reaction in cells and tissues

Metabolic conversion is a dynamic process that happens in living cells and tissues all the time, yet, the most adopted methods for measuring metabolism is though *in vitro* analysis of cell or tissue homogenates. High-speed SRS imaging platform opens the possibility to monitor metabolic conversions in real-time by probing chemical reactions *in situ*. By compositional mapping of lipid droplets in single living cells at the speed of 32 microseconds using multiplex SRS microscopy, intracellular metabolic conversion of retinoic acids into retinol was monitored in living cells [35] (Fig. 5). By developing hyperspectral SRS microscopy with high spectral resolution (9 cm^{-1}) and submicrometer spatial resolution, aromatic ring of lignin, aldehyde, and alcohol groups in lignified plant cell walls were spectrally and spatially separated [40]. By analysis of hyperspectral images with multivariate curve resolution, Liu et al. performed real-time monitoring of aldehyde reduction to alcohol in an intact plant tissue, which represents the lignin reduction. This work demonstrates the potential of SRS imaging in the understanding of dynamic lignin chemical compositions, which provides a novel technique for enhancing the efficiency of biomass utilization.

4. Probing chemical activities in living cells by SRS imaging of Raman probes

Molecules in biological samples contain chemical bonds that are spectrally overlapping. In order to study the transport or metabolism of a specific molecule, labeling the molecule of interest is helpful in some cases. Several chemical bonds, such as C–D, C≡C, and C≡N, give Raman signals in the silent region (1800–2800 cm^{-1}), which can be used to label specific molecules to track their trafficking and metabolism inside living cells and animals. These Raman tags are small, thus can be used to label small molecules with minimum perturbation of their biological functions, allowing bio-orthogonal chemical imaging in living cells and organisms.

The introduction of deuterium isotope in biological system has the advantage that it is stable without radioactivity and replacing hydrogen with deuterium does not change the molecular structure. Therefore, carbon-deuterium (C–D) bond has been used to label small molecules to study their uptake and metabolism in living cells and organisms. One example of the application of deuterated metabolite is visualizing *de novo* lipogenesis in living cells by feeding cells with deuterated glucose [55]. Compared to the currently

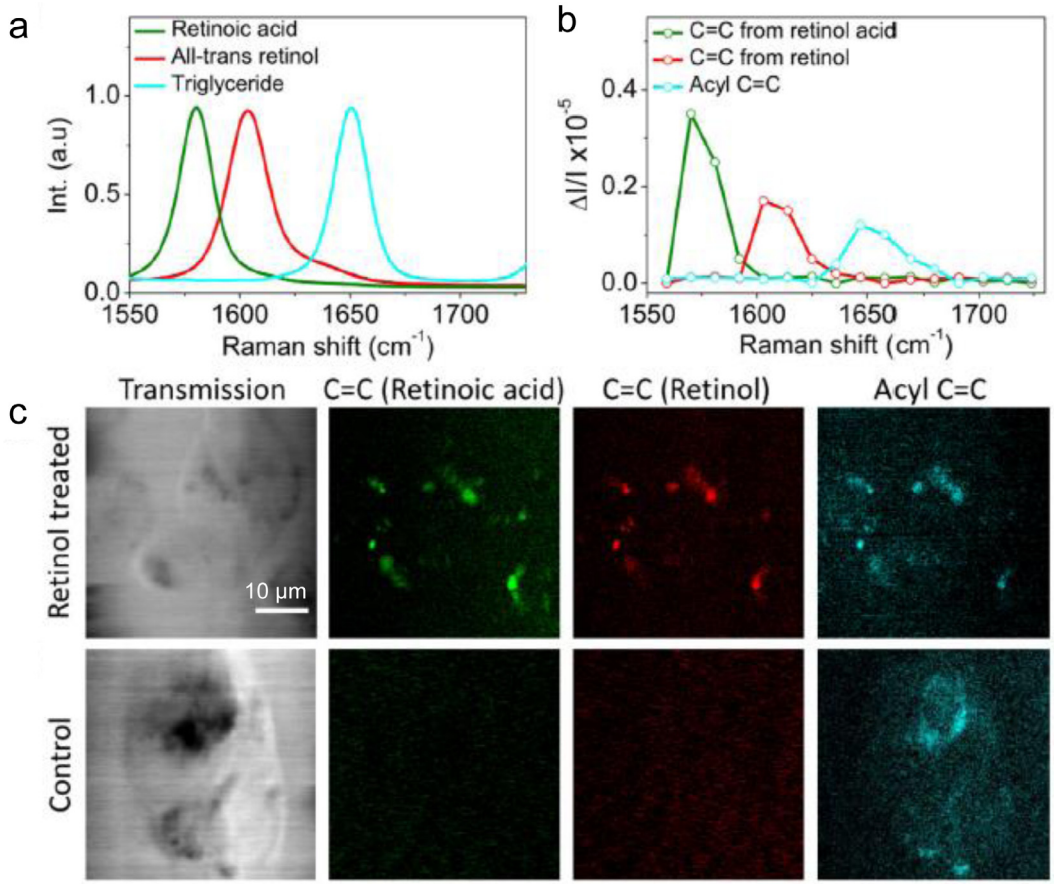

Fig. 5. Probing chemical reaction in cells and tissues. (a-c) monitoring intracellular metabolic conversion of retinoic acids into retinol. (a) Spontaneous Raman spectra. (b) MCR output spectra of all-trans retinol treated cancer cells imaged with multiplex SRS microscopy. (c) Transmission images and concentration maps of all-trans retinol treated cancer cells and control group imaged with multiplex SRS microscopy. Reprinted with permission from Ref. [35].

available glucose analogs, such as 3-O-methylglucose, 2-deoxy-D-glucose and fluoro-deoxyglucose, deuterated glucose can be metabolized by cells following the metabolic pathways, which allowed tracing of glucose to lipogenic fate in live cancer cells (Fig. 6a). *De novo* protein synthesis is another important process in biology that is visualized using deuterium labels [56,57]. Supplemented deuterated amino acids in the growth medium metabolically incorporate into translational machineries, providing enriched and specific C–D bond signals for newly synthesized proteins. By comparing with the endogenous protein Raman peak of Amide I band at 1655 cm^{-1} or CH_3 band at 2940 cm^{-1}, protein synthesis or degradation can be mapped in living cells [56] (Fig. 6b). Moreover, Raman peaks of C–D bonds vary slightly due to the structural differences. Taking advantage of these differences, two-color pulse-chase analysis of protein was designed to image formation of protein aggregates. Moving into *in vivo* imaging, this technique has been demonstrated in live brain tissues, zebrafish embryos and mice fed with deuterated amino acids [57]. In addition to glucose and amino acids, choline, a small molecule for membrane synthesis, neurotransmitter, and signaling pathway, has been imaged in living cells and *C. elegans* after metabolic incorporation of deuterated choline [58].

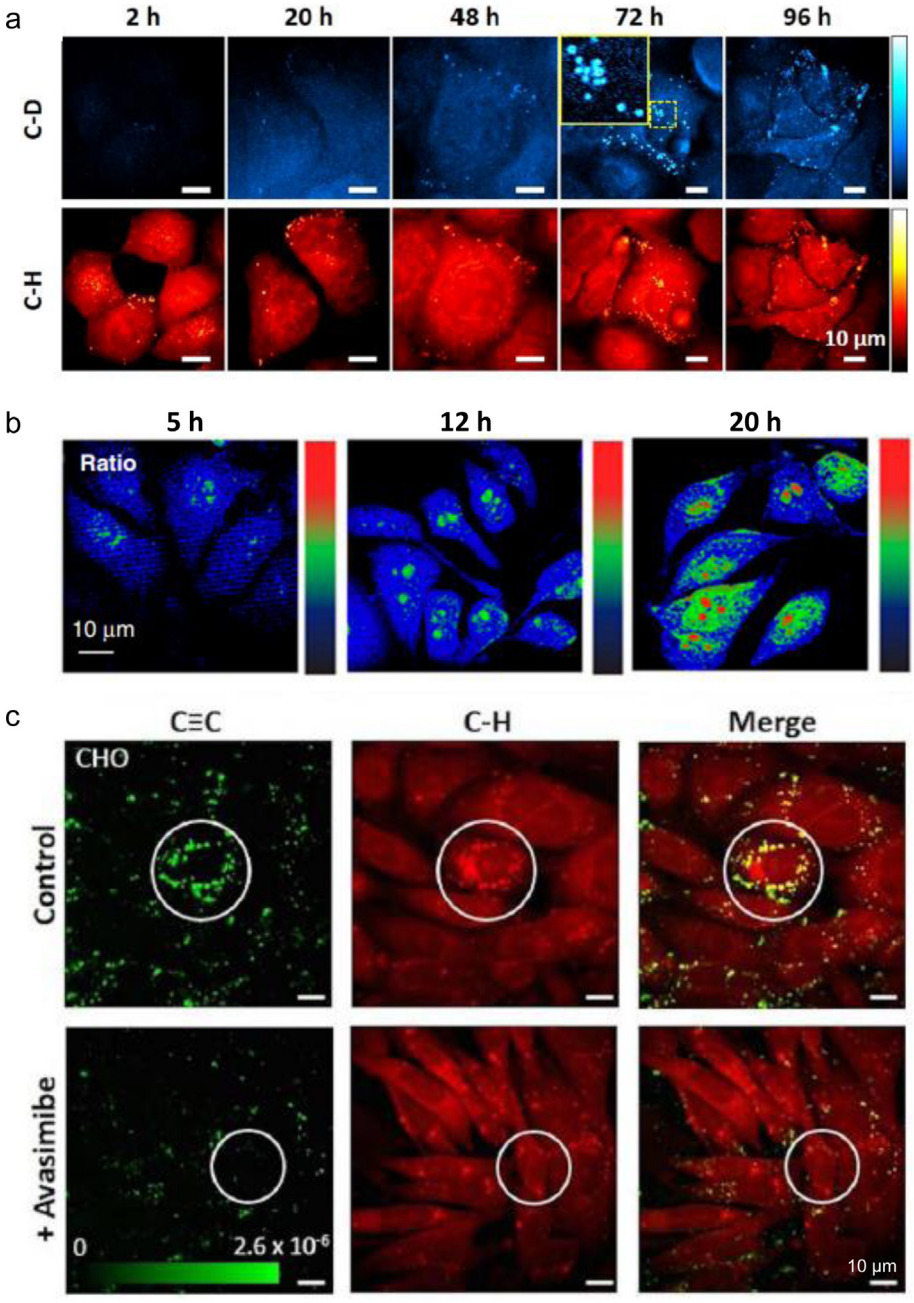

Fig. 6. Probing chemical activities in living cells by SRS imaging of Raman probes. (a) SRS imaging of pancreatic cancer PANC1 cells at C–D and C—H vibrations over time. Cells were treated with 25 mM glucose-d7 in glucose-free media supplemented with 10% FBS for times indicated in the figure. Reprinted with permission from Ref. [55]. (b) SRS imaging of *de novo* protein synthesis in HeLa cells incubated with deuterium-labeled all-amino acid medium. The ratio between SRS image at 2133 cm^{-1} (newly synthesized protein) and the SRS image at 1655 cm^{-1} (amide I band from total proteins) represents the relative new protein fraction at each time point. Reprinted with permission from Ref. [56]. (c) SRS images of phenyl-diyne cholesterol in CHO cells. Control cells show esterification and storage of phenyl-diyne cholesterol in lipid droplets. Inhibiting cholesterol esterification by avasimibe treatment reduced phenyl-diyne cholesterol storage in lipid droplets. Reprinted with permission from Ref. [66].

Lipids contain a number of C—H bonds that can be exchanged into C–D bonds, rendering various lipid species good candidates to be probed with SRS imaging of C–D bonds. Deuterated fatty acids were used to visualize cellular fatty acid uptake and distribution in lipid droplets and membranes [17]. By tracing deuterated saturated and unsaturated fatty acids in *C. elegans* using hyperspectral SRS imaging, Fu et al. identified different fates of these fatty acids upon uptake in the worms [59]. More recently, deuterated cholesterol was delivered into living cells to visualize cholesterol storage in steroidogenic cells [60].

As another important application of SRS imaging of C–D bonds *in vivo*, drug delivery to skin is studied using deuterated drug applied to animal and human skins. Deuterated DMSO was applied to human skin, and the penetration into the skin was visualized using epi-SRS imaging [41]. In another study, anti-inflammatory drug ketoprofen and ibuprofen was imaged in the mouse ear skin [61]. These studies show the potential of using SRS imaging technique to monitor dermato-pharmacokinetics in live animals and humans.

Although isotope labels provide biocompatible analogs for biological studies, the Raman scattering cross section of C–D bond vibration is relatively small. Alkyne bond (C≡C) has a Raman scattering cross-section that is larger than most endogenous chemical bonds [62,63]. The size of alkyne tag is small compared to a fluorescent dye, making it bio-orthogonal. Direct SRS imaging of a broad spectrum of alkyne-tagged small molecules, including deoxyribonucleosides, ribonucleosides, amino acids, choline, fatty acids and glycan, was demonstrated [63,64]. The reported SRS detection sensitivity for alkynes is around 200 μM with 100 μs pixel dwell time [63]. By feeding alkyne-tagged glucose to live tumor xenograft and brain tissues, glucose uptake was imaged using SRS imaging of alkyne bonds to study glucose uptake patterns [65]. In addition to biomolecules, alkyne tag has been proven to be an effective approach to image pharmacokinetics *in vivo*. Terbinafine hydrochloride, a FDA approved antifungal drug that contains alkyne bonds, was used to study the delivery of this skin drug to mouse ear tissue to ~100 μm depth [63].

Alkyne tag can be modified to further increase SRS signals and reduce cytotoxicity in some cases. Phenyl-diyne tagged cholesterol was designed to assess cholesterol storage in living cells and in *C. elegans* [66]. In this study, distribution of BODIPY-conjugated cholesterol is compared with phenyl-diyne cholesterol, showing that bulky and lipophilic BODIPY tag bypass metabolic process of cholesterol and move directly into lipid droplets, whereas bio-orthogonal phenyl-diyne cholesterol followed cholesterol esterification for storage [66] (Fig. 6c). It was shown that the Raman cross section of a phenyl-diyne tag is ~15 times higher than an alkyne tag, achieving the SRS detection limit of 30 μM phenyl-diyne cholesterol [66]. It should be noted that chirped femtosecond excitation was used to measure the detection limit of phenyl-diyne bond, whereas picosecond excitation was used to measure the detection limit of alkyne bond. In this study, probe size and SRS signal was carefully evaluated to achieve strong signal and biocompatibility, and the trade-off between these two parameters should be balanced in a case-by-case manner. Collectively, we expect that development of novel Raman tagged bio-orthogonal molecules will lead to better understanding of cellular processes by detecting specific chemical activities *in situ*.

5. Conclusions and outlook

With the capability of mapping chemical species in living cells and organisms in a label-free manner, SRS microscopy offers a novel platform to study metabolism, trafficking of organelles, and pharmacokinetics *in vivo*. The integration of SRS microscope and Raman tag provides an innovative strategy to map the metabolic activities of small molecules *in vivo*. We note that there are several limitations and/or disadvantages of current SRS imaging system. Raman scattering signals of endogenous chemical bonds are sometimes weak, resulting in low detection sensitivity. Also, the ability to distinguish chemical species may be compromised when there is no distinguishable vibrational signature due to similarities in chemical bonds. With these considerations in mind, we expect several promising directions in the future. The first direction is development of a broadband SRS microscope using an ultrashort pulse laser as excitation source. By covering the entire fingerprint vibration region, such a system would allow discovery of signatures inside living cells. The second direction is the study of less abundant metabolites enabled by further improving the sensitivity. Along this line, we anticipate novel design of Raman tagged small molecules for dynamic and functional study of biological processes. The third direction is the development of miniature SRS imaging systems, which have the penitential of clinical applications, for example, for diagnosis of cancer margin in the operating room.

Acknowledgements

This article is supported by a Keck Foundation Science & Engineering Grant, NIH R01GM118471, and DoD Award W81XWH-14-1-0557 to JXC.

References

[1] Y. Zhang, H. Hong, W. Cai, Imaging with Raman Spectroscopy, Curr. Pharm. Biotechnol. 11 (2010) 654–661.
[2] I. Georgakoudi, K.P. Quinn, Optical imaging using endogenous contrast to assess metabolic state, Annu. Rev. Biomed. Eng. 14 (2012) 351–367.
[3] A. Croce, G. Bottiroli, Autofluorescence spectroscopy and imaging: a tool for biomedical research and diagnosis, Eur. J. Histochem. (2014) 58.
[4] A.J. Walsh, R.S. Cook, M.E. Sanders, L. Aurisicchio, G. Ciliberto, C.L. Arteaga, M.C. Skala, Quantitative optical imaging of primary tumor organoid metabolism predicts drug response in breast cancer, Cancer Res. 74 (2014) 5184–5194.
[5] J.-X. Cheng, X.S. Xie, Coherent Raman Scattering Microscopy, CRC Press, Boca Raton, FL, 2012.
[6] C.L. Evans, X.S. Xie, Coherent anti-stokes Raman scattering microscopy: chemical imaging for biology and medicine, Annu. Rev. Anal. Chem. 1 (2008) 883–909.
[7] J.-X. Cheng, X.S. Xie, Coherent anti-stokes raman scattering microscopy: instrumentation, theory, and applications, J. Phys. Chem. B 108 (2004) 827.
[8] C.W. Freudiger, W. Min, B.G. Saar, S. Lu, G.R. Holtom, C. He, J.C. Tsai, J.X. Kang, X. S. Xie, Label-free biomedical imaging with high sensitivity by stimulated Raman scattering microscopy, Science 322 (2008) 1857–1861.
[9] D. Zhang, P. Wang, M.N. Slipchenko, J.X. Cheng, Fast vibrational imaging of single cells and tissues by stimulated Raman scattering microscopy, Acc. Chem. Res. 47 (2014) 2282–2290.
[10] W. Min, C.W. Freudiger, S. Lu, X.S. Xie, Coherent nonlinear optical imaging: beyond fluorescence microscopy, Annu. Rev. Phys. Chem. 62 (2011) 507–530.
[11] A.F. Palonpon, M. Sodeoka, K. Fujita, Molecular imaging of live cells by Raman microscopy, Curr. Opin. Chem. Biol. 17 (2013) 708–715.
[12] C.H.C. Jr, M.T. Cicerone, Chemically sensitive bioimaging with coherent Raman scattering, Nat. Photon. 9 (2015) 295–305.
[13] C. Krafft, I.W. Schie, T. Meyer, M. Schmitt, J. Popp, Developments in spontaneous and coherent Raman scattering microscopic imaging for biomedical applications, Chem. Soc. Rev. 45 (2016) 1819–1849.
[14] W.J. Tipping, M. Lee, A. Serrels, V.G. Brunton, A.N. Hulme, Chem Soc. Rev. 45 (2016) 2075–2089.
[15] L. Wei, F. Hu, Z. Chen, Y. Shen, L. Zhang, W. Min, Live-cell bioorthogonal chemical imaging: stimulated Raman scattering microscopy of vibrational probes, Acc. Chem. Res. 49 (2016) 1494–1502.
[16] R.C. Prince, R.R. Frontiera, E.O. Potma, Stimulated Raman scattering: from bulk to nano, Chem. Rev. 117 (2017) 5070–5094.
[17] D. Zhang, M.N. Slipchenko, J.X. Cheng, Highly sensitive vibrational imaging by femtosecond pulse stimulated Raman loss, J. Phys. Chem. Lett. 2 (2011) 1248–1253.
[18] D.J. Jones, E.O. Potma, J.-X. Cheng, B. Burfeindt, Y. Pang, J. Ye, X.S. Xie, Synchronization of two passively mode-locked, picosecond lasers within 20 fs for coherent anti-Stokes Raman scattering microscopy, Rev. Sci. Instrum. 73 (2002) 2843–2848.
[19] F. Ganikhanov, S. Carrasco, X. Sunney Xie, M. Katz, W. Seitz, D. Kopf, Broadly tunable dual-wavelength light source for coherent anti-Stokes Raman scattering microscopy, Opt. Lett. 31 (2006) 1292–1294.

[20] Y. Ozeki, F. Dake, S. Kajiyama, K. Fukui, K. Itoh, Analysis and experimental assessment of the sensitivity of stimulated Raman scattering microscopy, Opt. Express 17 (2009) 3651–3658.
[21] D. Zhang, M.N. Slipchenko, D.E. Leaird, A.M. Weiner, J.-X. Cheng, Spectrally modulated stimulated Raman scattering imaging with an angle-to-wavelength pulse shaper, Opt. Express 21 (2013) 13864–13874.
[22] M.N. Slipchenko, R.A. Oglesbee, D. Zhang, W. Wu, J.X. Cheng, Heterodyne detected nonlinear optical imaging in a lock-in free manner, J. Biophoton. 5 (2012) 801–807.
[23] J.L. Suhalim, C.Y. Chung, M.B. Lilledahl, R.S. Lim, M. Levi, B.J. Tromberg, E.O. Potma, Characterization of cholesterol crystals in atherosclerotic plaques using stimulated Raman scattering and second-harmonic generation microscopy, Biophys. J. 102 (2012) 1988–1995.
[24] J.C. Mansfield, G.R. Littlejohn, M.P. Seymour, R.J. Lind, S. Perfect, J. Moger, Label-free chemically specific imaging in planta with stimulated Raman scattering microscopy, Anal. Chem. 85 (2013) 5055–5063.
[25] D. Fu, G. Holtom, C. Freudiger, X. Zhang, X.S. Xie, Hyperspectral imaging with stimulated Raman scattering by chirped femtosecond lasers, J. Phys. Chem. B 117 (2013) 4634–4640.
[26] D. Fu, J. Zhou, W.S. Zhu, P.W. Manley, Y.K. Wang, T. Hood, A. Wylie, X.S. Xie, Imaging the intracellular distribution of tyrosine kinase inhibitors in living cells with quantitative hyperspectral stimulated Raman scattering, Nat. Chem. 6 (2014) 614–622.
[27] T. Hellerer, A.M.K. Enejder, A. Zumbusch, Spectral focusing: High spectral resolution spectroscopy with broad-bandwidth laser pulses, Appl. Phys. Lett. (2004) 85.
[28] D. Zhang, P. Wang, M.N. Slipchenko, D. Ben-Amotz, A.M. Weiner, J.X. Cheng, Quantitative vibrational imaging by hyperspectral stimulated Raman scattering microscopy and multivariate curve resolution analysis, Anal. Chem. 85 (2013) 98–106.
[29] K. Wang, D. Zhang, K. Charan, M.N. Slipchenko, P. Wang, C. Xu, J.X. Cheng, Time-lens based hyperspectral stimulated Raman scattering imaging and quantitative spectral analysis, J. Biophoton. 6 (2013) 815–820.
[30] Y. Ozeki, W. Umemura, Y. Otsuka, S. Satoh, H. Hashimoto, K. Sumimura, N. Nishizawa, K. Fukui, K. Itoh, High-speed molecular spectral imaging of tissue with stimulated Raman scattering, Nat. Photon. 6 (2012) 845–851.
[31] Y. Ozeki, W. Umemura, K. Sumimura, N. Nishizawa, K. Fukui, K. Itoh, Stimulated Raman hyperspectral imaging based on spectral filtering of broadband fiber laser pulses, Opt. Lett. 37 (2012) 431–433.
[32] B. Marx, L. Czerwinski, R. Light, M. Somekh, P. Gilch, Multichannel detectors for femtosecond stimulated Raman microscopy – ideal and real ones, J. Raman Spectrosc. 45 (2014) 521–527.
[33] F.K. Lu, M. Ji, D. Fu, X. Ni, C.W. Freudiger, G. Holtom, X.S. Xie, Multicolor stimulated Raman scattering (SRS) microscopy, Mol. Phys. 110 (2012) 1927–1932.
[34] K. Seto, Y. Okuda, E. Tokunaga, T. Kobayashi, Development of a multiplex stimulated Raman microscope for spectral imaging through multi-channel lock-in detection, Rev. Sci. Instrum. 84 (2013) 083705.
[35] C.-S. Liao, M.N. Slipchenko, P. Wang, J. Li, S.-Y. Lee, R.A. Oglesbee, J.-X. Cheng, Microsecond Scale Vibrational Spectroscopic Imaging by Multiplex Stimulated Raman Scattering Microscopy, Light Sci. Appl. 4 (2015) e265.
[36] D. Fu, F.K. Lu, X. Zhang, C. Freudiger, D.R. Pernik, G. Holtom, X.S. Xie, Quantitative chemical imaging with multiplex stimulated Raman scattering microscopy, J. Am. Chem. Soc. 134 (2012) 3623–3626.
[37] C.S. Liao, P. Wang, J. Li, H.J. Lee, G. Eakins, J.X. Cheng, Spectrometer-free vibrational imaging by retrieving stimulated Raman signal from highly scattered photons, Sci. Adv. 1 (2015) e1500738.
[38] D. Fu, X.S. Xie, Reliable cell segmentation based on spectral phasor analysis of hyperspectral stimulated Raman scattering imaging data, Anal. Chem. 86 (2014) 4115–4119.
[39] P. Wang, B. Liu, D. Zhang, M.Y. Belew, H.A. Tissenbaum, J.X. Cheng, Imaging lipid metabolism in live Caenorhabditis elegans using fingerprint vibrations, Angew. Chem. Int. Ed. Engl. 53 (2014) 11787–11792.
[40] B. Liu, P. Wang, J.I. Kim, D. Zhang, Y. Xia, C. Chapple, J.X. Cheng, Vibrational fingerprint mapping reveals spatial distribution of functional groups of lignin in plant cell wall, Anal. Chem. 87 (2015) 9436–9442.
[41] B.G. Saar, C.W. Freudiger, C.M. Stanley, G.R. Holtom, X.S. Xie, Video-rate molecular imaging in vivo with stimulated Raman scattering, Science 330 (2010) 1368–1370.
[42] M. Ji, D.A. Orringer, C.W. Freudiger, S. Ramkissoon, X. Liu, D. Lau, A.J. Golby, I. Norton, M. Hayashi, N.Y. Agar, G.S. Young, C. Spino, S. Santagata, S. Camelo-Piragua, K.L. Ligon, O. Sagher, X.S. Xie, Rapid, label-free detection of brain tumors with stimulated Raman scattering microscopy, Sci. Transl. Med. 5 (2013) 201–219.
[43] T.T. Le, H.M. Duren, M.N. Slipchenko, C.D. Hu, J.X. Cheng, Label-free quantitative analysis of lipid metabolism in living Caenorhabditis elegans, J. Lipid Res. 51 (2010) 672–677.
[44] M.C. Wang, W. Min, C.W. Freudiger, G. Ruvkun, X.S. Xie, RNAi screening for fat regulatory genes with SRS microscopy, Nat. Methods 8 (2011) 135–138.
[45] W. Dou, D. Zhang, Y. Jung, J.X. Cheng, D.M. Umulis, Label-free imaging of lipid-droplet intracellular motion in early Drosophila embryos using femtosecond-stimulated Raman loss microscopy, Biophys. J. 102 (2012) 1666–1675.
[46] X. Zhang, M.B. Roeffaers, S. Basu, J.R. Daniele, D. Fu, C.W. Freudiger, G.R. Holtom, X.S. Xie, Label-free live-cell imaging of nucleic acids using stimulated Raman scattering microscopy, Chem. Phys. Chem. 13 (2012) 1054–1059.
[47] C.R. Hu, D. Zhang, M.N. Slipchenko, J.X. Cheng, B. Hu, Label-free real-time imaging of myelination in the Xenopus laevis tadpole by in vivo stimulated Raman scattering microscopy, J. Biomed. Opt. 19 (2014) 086005.
[48] S. Yue, J. Li, S.-Y. Lee, H.J. Lee, T. Shao, B. Song, L. Cheng, T.A. Masterson, X. Liu, T.L. Ratliff, J.-X. Cheng, Cholesteryl ester accumulation induced by PTEN loss and PI3K/AKT activation underlies human prostate cancer aggressiveness, Cell Metab. 19 (2014) 393–406.
[49] J. Li, S. Condello, J. Thomes-Pepin, X. Ma, Y. Xia, T.D. Hurley, D. Matei, J.X. Cheng, Lipid desaturation is a metabolic marker and therapeutic target of ovarian cancer stem cells, Cell Stem Cell (2016).
[50] F.K. Lu, D. Calligaris, O.I. Olubiyi, I. Norton, W. Yang, S. Santagata, X.S. Xie, A.J. Golby, N.Y. Agar, Label-free neurosurgical pathology with stimulated Raman imaging, Cancer Res. 76 (2016) 3451–3462.
[51] P. Wang, J. Li, C.R. Hu, D. Zhang, M. Sturek, J.X. Cheng, Label-free quantitative imaging of cholesterol in intact tissues by hyperspectral stimulated Raman scattering microscopy, Angew. Chem. Int. Ed. Engl. 52 (2013) 13042–13046.
[52] C.W. Freudiger, R. Pfannl, D.A. Orringer, B.G. Saar, M. Ji, Q. Zeng, L. Ottoboni, W. Ying, C. Waeber, J.R. Sims, P.L. De Jager, O. Sagher, M.A. Philbert, X. Xu, S. Kesari, X.S. Xie, G.S. Young, Multicolored stain-free histopathology with coherent Raman imaging, Lab Invest. 92 (2012) 1492–1502.
[53] E.J. O'Rourke, A.A. Soukas, C.E. Carr, G. Ruvkun, *C. elegans* major fats are stored in vesicles distinct from lysosome-related organelles, Cell Metab. 10 (2009) 430–435.
[54] H.Y. Mak, Lipid droplets as fat storage organelles in Caenorhabditis elegans: Thematic Review Series: Lipid Droplet Synthesis and Metabolism: from Yeast to Man, J. Lipid Res. 53 (2012) 28–33.
[55] J. Li, J.-X. Cheng, Direct visualization of de novo lipogenesis in single living cells, Sci. Rep. 4 (2014) 6807.
[56] L. Wei, Y. Yu, Y. Shen, M.C. Wang, W. Min, Vibrational imaging of newly synthesized proteins in live cells by stimulated Raman scattering microscopy, Proc. Natl. Acad. Sci. U. S. A. 110 (2013) 11226–11231.
[57] L. Wei, Y. Shen, F. Xu, F. Hu, J.K. Harrington, K.L. Targoff, W. Min, Imaging complex protein metabolism in live organisms by stimulated Raman scattering microscopy with isotope labeling, ACS Chem. Biol. 10 (2015) 901–908.
[58] F. Hu, L. Wei, C. Zheng, Y. Shen, W. Min, Live-cell vibrational imaging of choline metabolites by stimulated Raman scattering coupled with isotope-based metabolic labeling, Analyst 139 (2014) 2312–2317.
[59] D. Fu, Y. Yu, A. Folick, E. Currie, R.V. Farese Jr., T.H. Tsai, X.S. Xie, M.C. Wang, In vivo metabolic fingerprinting of neutral lipids with hyperspectral stimulated Raman scattering microscopy, J. Am. Chem. Soc. 136 (2014) 8820–8828.
[60] A. Alfonso-Garcia, S.G. Pfisterer, H. Riezman, E. Ikonen, E.O. Potma, D38-cholesterol as a Raman active probe for imaging intracellular cholesterol storage, J. Biomed. Opt. 21 (2016) 61003.
[61] B.G. Saar, L.R. Contreras-Rojas, X.S. Xie, R.H. Guy, Imaging drug delivery to skin with stimulated Raman scattering microscopy, Mol. Pharm. 8 (2011) 969–975.
[62] H. Yamakoshi, K. Dodo, A. Palonpon, J. Ando, K. Fujita, S. Kawata, M. Sodeoka, Alkyne-tag Raman imaging for visualization of mobile small molecules in live cells, J. Am. Chem. Soc. 134 (2012) 20681–20689.
[63] L. Wei, F. Hu, Y. Shen, Z. Chen, Y. Yu, C.C. Lin, M.C. Wang, W. Min, Live-cell imaging of alkyne-tagged small biomolecules by stimulated Raman scattering, Nat. Methods 11 (2014) 410–412.
[64] S. Hong, T. Chen, Y. Zhu, A. Li, Y. Huang, X. Chen, Live-cell stimulated Raman scattering imaging of alkyne-tagged biomolecules, Angew. Chem. Int. Ed. Engl. 53 (2014) 5827–5831.
[65] Y. Shen, F. Xu, L. Wei, F. Hu, W. Min, Live-cell quantitative imaging of proteome degradation by stimulated Raman scattering, Angew. Chem. Int. Ed. Engl. 53 (2014) 5596–5599.
[66] H.J. Lee, W. Zhang, D. Zhang, Y. Yang, B. Liu, E.L. Barker, K.K. Buhman, L.V. Slipchenko, M. Dai, J.X. Cheng, Assessing Cholesterol Storage in Live Cells and C. elegans by Stimulated Raman Scattering Imaging of Phenyl-Diyne Cholesterol, Sci. Rep. 5 (2015) 7930.